

High-efficiency AlGaInP/AlGaAs vertical-cavity surface-emitting lasers with 650 nm wavelength

A. Knigge, M. Zorn, J. Sebastian, K. Vogel, H. Wenzel, M. Weyers and G. Tränkle

Abstract: The optimisation of red, AlGaInP/AlGaAs-based, selectively oxidised vertical-cavity surface-emitting lasers (VCSELs) with 650 nm emission wavelength having all-semiconductor p-distributed Bragg reflectors is reported. The increase of the AlP content in parts of the cavity, tailoring of the doping profile and removal of the contact layer in the output window lead to VCSELs with threshold current densities of 1.8 kA/cm^2 and continuous wave output powers of 3.1 mW to 4.6 mW at 20°C for wavelengths between 650 nm and 657 nm. These devices with current apertures around $13 \mu\text{m}$ show laser emission above temperatures of 40°C ; devices with smaller apertures and room temperature output powers of 1 mW show laser emission up to 60°C .

1 Introduction

High-performance visible-wavelength vertical-cavity surface-emitting lasers (VCSELs) in the wavelength region near 650 nm are needed for emerging technologies such as high-density optical storage systems, high-definition laser printing and especially optical communication systems based on plastic optical fibres, for which absorption losses have a minimum at 650 nm. Furthermore, visible VCSELs can be used directly, for example in laser visors or for distance measurements. In this case eye sensitivity and eye safety demand wavelengths of 650 nm or less, output powers of 1 mW maximum and operating temperatures up to 50°C . While high-performance near-IR (In)GaAs/AlGaAs VCSELs are commercially available, there are only a few publications concerning AlGaInP-based VCSELs with wavelengths near 650 nm. In 1996, Choquette *et al.* [1] reported a continuous-wave (CW) output power of 0.28 mW for 652 nm, but there was no breakthrough in following years. In 2000, they reported a single-mode maximum output power of 0.4 mW at 650 nm [2]. Most of the other groups investigated VCSELs with longer wavelengths, e.g. 667 nm with a multimode output power of 2.0 mW [3] or even longer wavelengths up to 690 nm [4]. However, the maximum output is known to decrease drastically with decreasing wavelength.

To our knowledge, the highest VCSEL output power of 2 mW at 650 nm was reported in [5]. In contrast to [1–4], VCSELs presented there are not realised with all-semiconductor p-distributed Bragg reflectors (DBR). The upper part of the p-DBR consisted of four pairs of AlGaInP/AlAs, where the AlAs is completely oxidised to native Al oxide. Unfortunately, these devices operated CW only at temperatures up to 25°C .

The poor temperature stability of the red VCSEL material is discussed in [6] for VCSELs with all-semiconductor oxidised p-DBRs and in [7] for implanted VCSELs. Both show laser emission up to 60°C for devices with 666 nm room temperature laser wavelength.

In this paper, the optimisation of AlGaInP-based, selectively oxidised VCSELs with wavelengths close to 650 nm with all-semiconductor p-DBRs is reported, especially improvement due to the introduction of an additional bandgap step in the resonator cavity. The optimisation of the doping profile and the removal of the contact layer in the output window double the room temperature output power. The size of the current aperture influences the CW output power and the maximum operating temperature.

2 Sample preparation and measurement details

The AlGaInP/AlGaAs-based heterostructures were grown in a low-pressure metalorganic vapour phase epitaxy (MOVPE) system AIXTRON 200/4 with in-situ growth control [8] and standard sources (trimethylgallium, trimethylaluminium, trimethylindium, arsine, phosphine). Trimethylgallium is used to grow $\text{Al}_x\text{Ga}_{1-x}\text{As}$ with $0.95 \leq x < 1$. Si from disilane was used as n-dopant, and Zn from diethylzinc in AlGaInP and intrinsically incorporated carbon in AlGaAs as p-dopants. The latter was achieved by growth at low V/III ratios. $(100) \text{ n}^+ \text{ GaAs}$ substrates misoriented 6° towards $[111] \text{ A}$ were used [9].

VCSELs presented in this paper have three compressively strained GaInP quantum wells (QWs) embedded in a $1 - \lambda$ optical cavity (see Fig 1). In sample A the QW barriers and the spacer layers have the same composition $\text{Al}_{0.26}\text{Ga}_{0.26}\text{In}_{0.48}\text{P}$. In samples B and C the spacer layers consist of $\text{Al}_{0.35}\text{Ga}_{0.17}\text{In}_{0.48}\text{P}$. QWs and barriers are nominally undoped. The room temperature electroluminescence spectrum of the QWs has its maximum at 645 nm. The cavity is surrounded by quarter-wave $\text{Al}_{0.5}\text{Ga}_{0.5}\text{As}/\text{Al}_x\text{Ga}_{1-x}\text{As}$ distributed Bragg reflectors (DBR). The Si-doped bottom mirror has $55\frac{1}{2}$ pairs with $x = 1.0$. Its $\text{Al}_{0.5}\text{Ga}_{0.5}\text{As}-\text{AlAs}$ interfaces are abrupt in sample A and B and linearly graded in sample C. The carbon-doped top mirror has 35 pairs with $x = 0.95$ and

© IEE, 2003

IEE Proceedings online no. 20030372

DOI: 10.1049/ip-opt:20030372

Paper first received 22nd January and in revised form 5th July 2002

The authors are with the Ferdinand-Braun-Institut für Höchstfrequenztechnik, Albert-Einstein-Straße 11, 12489 Berlin, Germany

	Sample A	Sample B	Sample C	Sample D
p-contact	Ti/Pt/Au			
contact layer	p-GaAs			partially removed
etch stop layer	-			p-InGaP
35 × p-DBR	Al _{0.5} Ga _{0.5} As/Al _{0.95} Ga _{0.05} As, graded interfaces		+ δ-doping + increasing doping	
spacer	p-Al _{0.26} Ga _{0.26} In _{0.48} P	p-Al _{0.35} Ga _{0.17} In _{0.48} P		
barrier	Al _{0.26} Ga _{0.26} In _{0.48} P			
3 QWs	compressively strained InGaP (λ = 645 nm)			
barrier	Al _{0.26} Ga _{0.26} In _{0.48} P			
spacer	n-Al _{0.26} Ga _{0.26} In _{0.48} P	n-Al _{0.35} Ga _{0.17} In _{0.48} P		
55.5 × n-DBR	Al _{0.5} Ga _{0.5} As/AlAs, abrupt interfaces		graded interfaces	
substrate	n-GaAs 6° to {111} A			
n-contact	Ge/Au/Ni/Au			

Fig. 1 Layer sequence of laser structures under investigation

graded interfaces. For selective oxidation the third p-DBR pair above the cavity has $x = 0.98$. In the p-DBR of sample C an additional pulse doping is added together with an increase in the doping level from the cavity to the contact layer. Sample D has a 10 nm thick InGaP etch stop layer in the last p-DBR layer under the p-GaAs contact layer. Owing to the intended growth rate profile along the wafer radius the cavity resonance wavelength shifts about 30 nm from the middle to the edge of the wafers.

Air-post mesa structures of 30 μm to 60 μm diameter, so-called broad area VCSELs, were processed using standard photolithography and BCl₃/Ar plasma etching of the top DBR. On top of the mesa there is an 8 μm wide metallised ring that serves as p-side contact and also defines the light emission window. In sample D the contact layer is wet etched down to the etch stop layer, which simultaneously passivates the underlying p-DBR layer with its high aluminium content. In a subsequent processing step a current aperture is introduced by selective wet oxidation into the third p-DBR pair using the oxidation rate difference between Al_{0.98}Ga_{0.02}As and Al_{0.95}Ga_{0.05}As [10].

Electrical and optical characterisation was done in pulsed and CW operation by direct wafer probing. In pulsed operation (pulse width 200 ns, duty cycle 1:1000) broad area VCSELs were measured at room temperature (RT = 20°C). In CW operation devices with mesa diameters of 35 to 45 μm and oxide apertures with diameters of 5 to 17 μm were tested at temperatures between 10°C and 60°C. In both operating modes power/current and voltage/current characteristics and emission spectra were measured.

3 Results and discussion

3.1 Broad area devices in pulsed operation

For process-independent evaluation of the epitaxial layer design power/current characteristics and emission spectra of broad area VCSELs (diameter 60 μm) without wet

oxidised current apertures were measured in pulsed operation in the radial direction on each wafer. From these measurements the threshold current density (j_{th}) and the output power at a current of 350 mA was determined for all samples A–D and plotted against the laser wavelength (Fig. 2). The threshold current density has a strong minimum and the output power has a strong maximum. To adjust the threshold current density minimum at 650 nm the maximum of the room temperature electroluminescence of the QW was tuned to be at 645 nm. For wavelengths below and above 650 nm the threshold current density increases due to detuning between the QW gain and the cavity resonance. The threshold current density increases with decreasing wavelength due to current leakage, which is more pronounced at smaller wavelengths [6].

Fig. 2 shows the strong change of device properties for sample B compared to sample A due to the change of spacer layer composition: the threshold current density at 650 nm of 5.3 kA/cm² in sample A is reduced to 2.3 kA/cm² in sample B. The output power is nearly doubled. To understand this, the profile of the band edges of sample A and B are depicted in Fig. 3. The introduction of the Al_{0.35}Ga_{0.17}In_{0.48}P spacer layer seems to enhance carrier confinement in the QWs compared to sample A because there are additional band offsets for holes and electrons at the Γ point between spacer and barriers in sample B. Consequently the leakage of these carriers into the corresponding DBRs is diminished. Furthermore, both the AlGaAs DBRs and the Al_{0.35}Ga_{0.17}In_{0.48}P spacer layers are indirect semiconductors with the minimum of the conduction band at the X valley, while the Al_{0.26}Ga_{0.26}In_{0.48}P barriers and the InGaP QWs are direct semiconductors. This may improve carrier injection from the DBRs into the QWs. Moreover, the minority carrier lifetime in the indirect spacer layers should be enhanced, which reduces the recombination current outside of the QWs additionally in sample B.

For further improvement of the laser performance the series resistance was reduced in sample C by grading the AlGaAs–AlAs interfaces also in the n-DBR, by

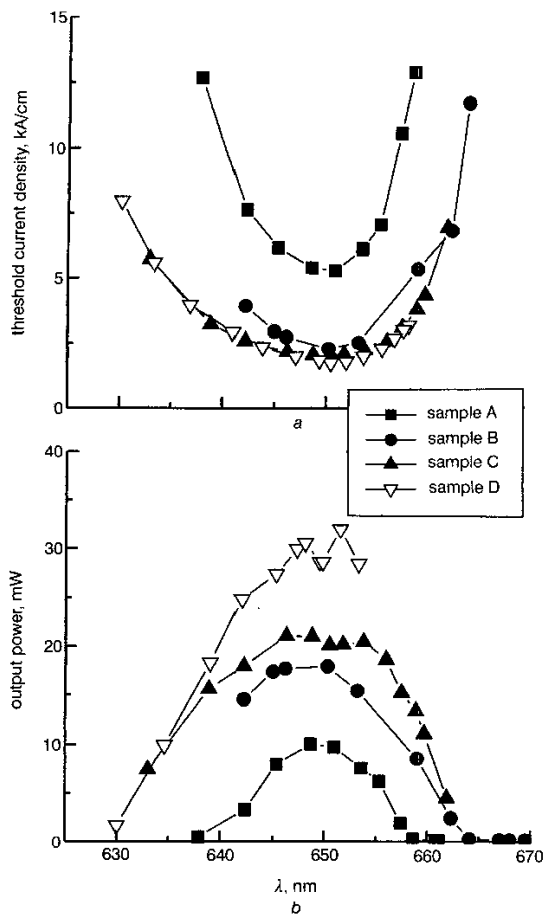


Fig. 2 Threshold current density (a) and output power at 350 mA (b) against emission wavelength for 60 μm VCSELs without current apertures at room temperature in pulsed operation (200 ns, 1:1000)

introducing pulse doping in the p-DBR and by an increasing doping level through the p-DBR towards the contact layer. As a result, the threshold current density is further diminished and the maximum output power is increased. At 7 kA/cm² and 650 nm an output power as high as 21 mW is obtained in pulsed operation.

The output power in sample D is even higher. Its p-GaAs contact layer is removed by selective etching down to the InGaP etch stop layer, which also passivates the underlying p-DBR layers with high aluminium content. The minimum of the threshold current density is as low as 1.8 kA/cm² and the maximum pulsed output power at 7 kA/cm² is increased to 31 mW. This improvement is caused by the elimination of absorption in the highly p-doped GaAs contact layer with its bandgap energy (1.42 eV) below the photon energy $E = 1.91$ eV corresponding to $\lambda = 650$ nm. There was neither a change in the modal structure nor an increase in the series resistance without the GaAs contact layer, which may serve as a current spreading layer.

3.2 Oxide aperture VCSELs in CW operation

To obtain CW operation, an aperture was generated in the broad area VCSELs by selective wet oxidation. Fig. 4 shows CW power/current characteristics of devices with emission wavelengths of 650 nm and 654 nm. At room temperature, CW operation was obtained from VCSELs of

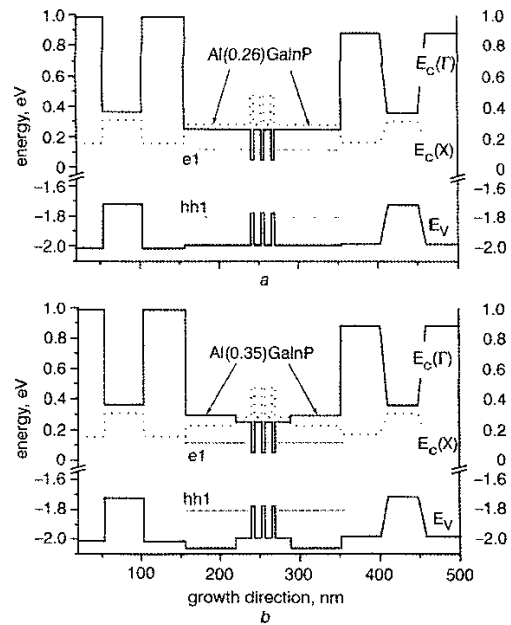


Fig. 3 Band edge profiles of the inner VCSEL structure
 E_c : conduction band at Γ -point (solid line) and X-point (dotted line);
 E_v : heavy hole valence band; e1: 1. electron state; hh1: 1. heavy hole state (dashed lines)
 a Sample A; b sample B

sample A with small aperture sizes only and wavelengths between 650 nm and 658 nm. The 650 nm device emitted 160 μW at 3.8 mA with a threshold current of 1.7 mA. At 10°C the output power was 400 μW and laser emission occurred over a wider wavelength range (647–660 nm; Fig. 5). Devices with apertures larger than 10 μm do not lase in CW operation, not even at 10°C.

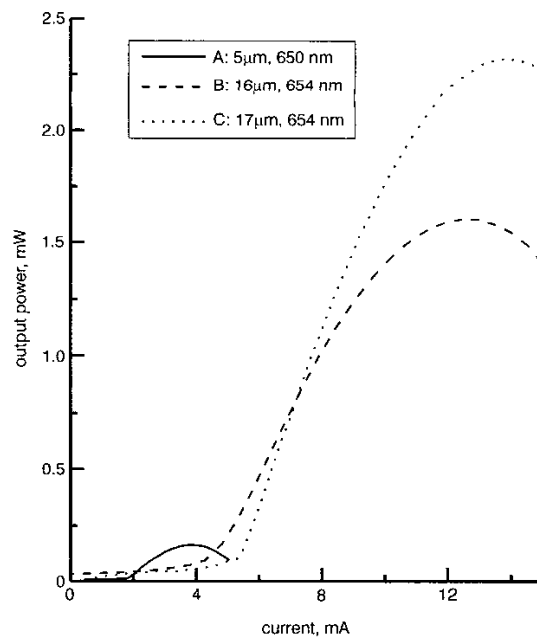


Fig. 4 CW power/current characteristics at 20°C of samples A, B and C with oxide aperture diameters of 5, 16 and 17 μm , respectively

Wavelengths: A: 650 nm, B and C: 654 nm

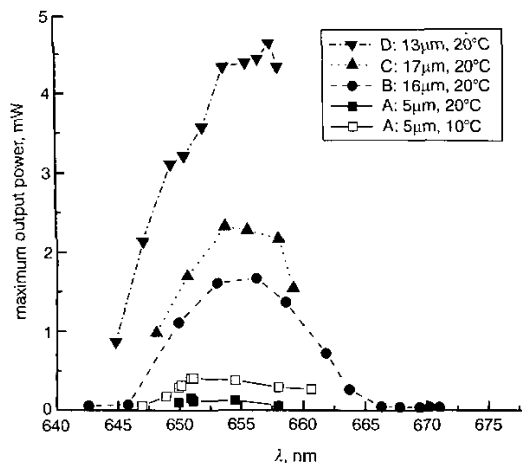


Fig. 5 Maximum CW output power in dependence on the laser wavelength at 10°C and 20°C for samples A to D

As expected from the pulsed laser data, the CW lasing performance of VCSELs from sample B is much better than those of sample A: laser emission is obtained not only from devices with small current aperture sizes (about 5 μm) but also from aperture sizes up to 16 μm. At 20°C laser operation is achieved in the wavelength range between 646 nm and 664 nm (Fig. 5). The maximum output power of 1.6 mW at 20°C and 2.8 mW at 10°C is reached at 653 nm. Even higher output powers are obtained from sample C with the improved doping profile. The 653 nm device with a 17 μm wide aperture emits 2.3 mW at room temperature and 3.7 mW at 10°C.

Comparing the wavelength dependence of the pulsed output power at constant current (Fig. 2b) and the maximum CW output power (Fig. 5) of sample B and C shows a wavelength shift of about 6 nm. This red shift results from the interaction of the gain shift due to heating and increasing leakage current. The latter is much more pronounced with decreasing wavelength, increasing temperature and operating current.

The highest output power is obtained from sample D with removed contact layer in the output window and 13 μm wide apertures (Fig. 6). The maximum output power is 3.1 mW at λ = 650 nm and higher than 4 mW at λ = 654 nm in multimode emission. These values are clearly higher than the reported 0.4 mW at 650 nm for all-semiconductor DBRs [2], even considering single-mode emission, and the reported 2 mW from multimode VCSELs with partly native oxide DBRs [5]. With operating voltages between 2 V and 3 V the peak wall-plug efficiency reaches 15% at λ = 650 nm and 16% at λ = 654 nm. The maximum differential external efficiency is 38%, little above threshold (λ = 654 nm). The comparison of VCSEL characteristics of samples C and D in Fig. 6 emphasises the significant benefit of the removal of the highly p-doped GaAs contact layer in the output window.

For low-cost applications without temperature stabilisation, laser operation at elevated temperatures is required. Power-current characteristics up to 60°C show a strong output power decrease with increasing heat sink temperature. 650 nm VCSELs from sample C with large aperture sizes (16 μm) show a maximum output power of 3.2 mW at 10°C, at room temperature this is nearly halved and at 35°C there is no laser emission at all (Fig. 7). More than 10 K higher operating temperatures are obtained with

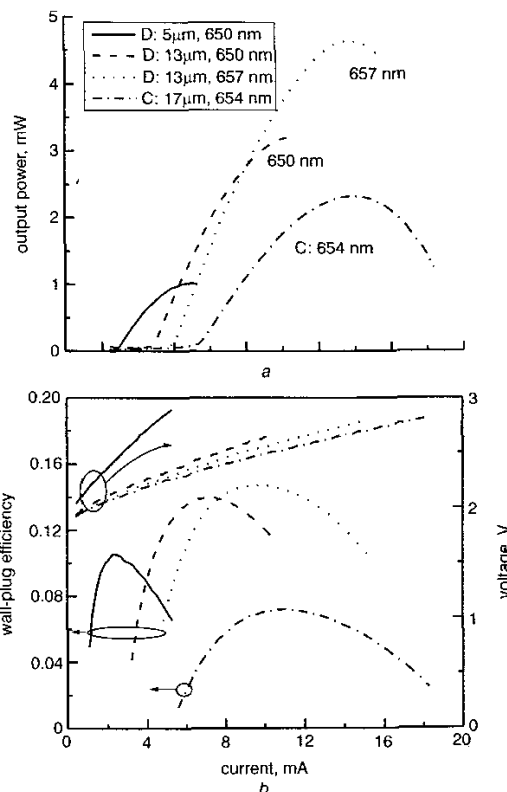


Fig. 6 Characteristics at 20°C of samples C and D with oxide aperture diameters of 5, 13 and 17 μm

a CW power against current
b Wall-plug efficiency and voltage against current

VCSELs from sample D: devices with 13 μm wide apertures and λ = 650 nm lase up to 35°C; devices with λ = 657 nm up to 40°C. Even higher operating temperatures are obtained from VCSELs with smaller apertures. As can be seen in Fig. 7, the 651 nm device with 6 μm aperture shows laser operation up to 50°C. Its 20°C output power is smaller than that of the larger devices, but it is higher for temperatures above 40°C. Its output power at 45°C is still

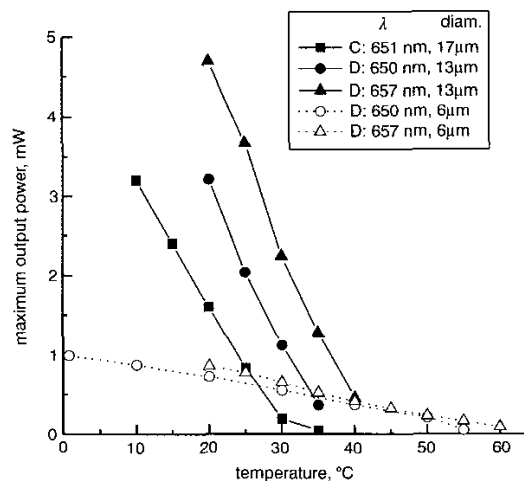


Fig. 7 Temperature dependence of the maximum CW output power from samples C and D with 6 to 17 μm aperture size

160 μ W, but at 50°C, only 30 μ W. VCSELs with 5 μ m aperture and $\lambda = 657$ nm show laser operation up to 60°C.

Evaluation of the threshold current dependence on temperature shows that the threshold current increase with temperature is much higher for VCSELs with large apertures than with small apertures. The threshold current of the device with a 13 μ m aperture and $\lambda = 657$ nm, whose power dependence on temperature is shown in Fig. 7, increases considerably with temperatures above 25°C, whereas the device with 6 μ m aperture shows only a very slight increase in the threshold current up to 55°C.

The dependence of maximum output power on the diameter of the oxide aperture can be explained as follows. In order to facilitate high-temperature operation, the temperature rise within the active region at threshold should be as small as possible. Because the dissipated thermal power increases with the active area, simulations have shown [11] that the temperature within the active area increases too, despite the decrease in thermal resistance with increasing oxide aperture. Note, however, that if the active area is too small, the temperature rises again, due to the strong increase in threshold current density.

4 Summary

A marked improvement in the properties of red VCSELs for 650 nm has been achieved by an increase of the AlP content in parts of the cavity. In pulsed operation, the threshold current density of VCSELs with an $\text{Al}_{0.35}\text{Ga}_{0.17}\text{In}_{0.48}\text{P}/\text{Al}_{0.26}\text{Ga}_{0.26}\text{In}_{0.48}\text{P}$ cavity is only half the value of VCSELs with a pure $\text{Al}_{0.26}\text{Ga}_{0.26}\text{In}_{0.48}\text{P}$ cavity. Furthermore, the pulsed output power is nearly twice as high. With a homogeneous cavity, room temperature CW operation is obtained only in small devices with output powers in the 100 μ W range and in a small wavelength window. Devices with a stepped cavity show laser operation also with aperture diameters up to 16 μ m and have output powers higher than 1 mW. Even higher room temperature output powers up to 4.6 mW are achieved with an optimised doping profile and removed contact layer.

Although the CW room temperature output power of large VCSELs reaches several milliwatts and wall plug efficiencies of 16%, the operating temperature is limited to 40°C. Higher temperatures up to 60°C are possible with smaller apertures. With 1 mW room temperature output power, such 657 nm devices emit 90 μ W at 60°C.

A further increase of output power at elevated temperatures requires the optimisation of aperture diameters and improved heat removal, for example by galvanic airbridges.

5 Acknowledgments

The authors would like to thank O. Fink for technical assistance with the MOVPE system and W. John, and U. Zeimer for support during the process development. The work was supported by the Deutsche Forschungsgemeinschaft (DFG) under contract Tr 357-1/2.

6 References

- 1 CHOQUETTE, K.D., SCHNEIDER, R.P., HAGEROTT CRAWFORD, M., GEIB, K.M., and FIGIEL, J.J.: 'Continuous wave operation of 640-660 nm selectively oxidized AlGaInP vertical-cavity lasers', *Electron. Lett.*, 1995, **31**, pp.1145-1156
- 2 CHOQUETTE, K.D., HAFICH, M.J., HAGEROTT CRAWFORD, M., GEIB, K.M., and HINDI, J.J.: 'Improved performance of selectively oxidized visible VCSELs'. Proceedings of LEOS '99, IEEE Lasers and Electro-Optics Society 1999 12th Annual meeting, 1999, **2**, pp.395-396
- 3 LAMBKIN, J.D., CALVERT, T., WOODHEAD, J., PINCHES, S.M., ONISCHENKO, A., SALE, T.E., HOSEA, J., VAN DAELE, P., VANDEPUTTE, K., VAN HOVE, A., VALSTER, A.D., MCINERNEY, J.G., and PORTA, P.A.: 'Development of a red VCSEL-to-plastic fiber module for use in parallel optical data links', *Proc. SPIE-Int. Soc. Opt. Eng.*, 2000, **3946**, pp.95-107
- 4 SAARINEN, M., TOIVONEN, M., XIANG, N., VILOKKINEN, V., and SAARINEN, M.: 'Room-temperature CW operation of red vertical-cavity surface-emitting lasers grown by solid-source molecular beam epitaxy', *Electron. Lett.*, 2000, **36**, (14), pp.1210-1211
- 5 LOTT, J.A., BUYDENS, L.V., MALLEY, K.J., KOBAYASHI, K., and ISHIKAWA, S.: 'Visible (630-650 nm) vertical cavity surface emitting lasers with Al-oxide/AlGaInP/AlGaAs distributed Bragg reflectors', *Inst. Phys. Conf. Ser.*, 1996, **145**, pp.973-976
- 6 KNOWLES, G., SWEENEY, S.J., and SALE, T.: 'Influence of leakage and gain-cavity alignment on the performance of Al(GaInP) visible vertical-cavity surface-emitting lasers', *IEE Proc., Optoelectron.*, 2001, **148**, (1), pp.55-59
- 7 TAKAOKA, K., ISHIKAWA, M., and HATAKOSHI, G.: 'Low-threshold and high-temperature operation of InGaAlP-based proton-implanted red VCSELs', *IEEE J. Sel. Top. Quantum Electron.*, 2001, **7**, (2), pp.381-385
- 8 ZORN, M., HABERLAND, K., KNIGGE, A., BHATTACHARYA, A., WEYERS, M., ZETTLER, J.-T., and RICHTER, W.: 'MOVPE process development for 650 nm VCSELs using optical in-situ techniques', *J. Cryst. Growth*, 2002, **235**, pp.25-34
- 9 BHATTACHARYA, A., ZORN, M., OSTER, A., NASAREK, M., WENZEL, H., SEBASTIAN, J., WEYERS, M., and TRÄNKLE, G.: 'Optimization of MOVPE growth for 650 nm-emitting VCSELs', *J. Cryst. Growth*, 2000, **221**, pp.663-667
- 10 ASHBY, C.I.H., BRIDGES, M.M., ALLERMANN, A.A., HAMMONS, B.E., and HOU, H.Q.: 'Origin of the time dependence of wet oxidation of AlGaAs', *Appl. Phys. Lett.*, 1999, **75**, pp.73-75
- 11 PIPREK, J.: 'High-temperature lasing of long-wavelength VCSELs: problems and prospects', *Proc. SPIE-Int. Soc. Opt. Eng.*, 1997, **3003**, pp.182-193